

Energy-Aware Dynamic Trajectory Planning for UAV-Enabled Data Collection in mMTC Networks

Lingfeng Shen, Ning Wang¹, Member, IEEE, Di Zhang², Senior Member, IEEE, Jun Chen³, Senior Member, IEEE, Xiaomin Mu, Member, IEEE, and Kon Max Wong, Life Fellow, IEEE

Abstract—A fundamental design problem for massive machine-type communication (mMTC) networks is efficient data collection from the machine-type communication devices (MTCs), which is the subject of investigation in this paper. An unmanned aerial vehicle (UAV) being deployed to facilitate data collection from MTCs is considered. Taking into account the limited energy for both the UAV and MTCs, a problem of minimizing the total energy consumption subject to completion of the data collection tasks by planning the UAV trajectory is formulated. A Global Optimum (GOP) trajectory can be obtained for a UAV serving all the MTCs simultaneously if the UAV's flying altitude is larger than $\sqrt{3}$ times its maximum service radius. However, communication energy efficiency drops as the UAV's altitude increases. Clustering-based service strategies and dynamic trajectory planning algorithms, namely clustered GOP (C-GOP) and clustered particle swarm optimization (C-PSO), are proposed to overcome the above issue. The data collection efficiency is maximized by locating the optimal UAV hovering point for each serving MTC cluster, which is dynamically adjusted with the UAV hovering position until all MTCs are served. It is shown that the GOP is the optimal strategy for a small number of MTCs concentrated in a small area. While for large number of MTCs or task area, the clustered algorithms are more favorable from energy efficiency, complexity and scalability perspectives.

Index Terms—Dynamic trajectory planning, energy efficiency, massive machine-type communications, UAV-enabled data collection.

Manuscript received 12 March 2022; revised 28 May 2022; accepted 18 June 2022. Date of publication 28 June 2022; date of current version 22 November 2022. This work was supported in part by the National Natural Science Foundation of China (NSFC) under Grant 61771431 and Grant 62001423; in part by the Henan Province Key Science and Technology Project under Grant 202102210328; and in part by the Zhengzhou Major Projects of Scientific and Technological Innovation under Grant 2020CXZX0080. This article was presented in part at the 2020 IEEE 92nd Vehicular Technology Conference (VTC2020-Fall), 2020, pp. 1–6 [DOI: 10.1109/VTC2020-Fall49728.2020.9348455]. The editor coordinating the review of this article was P. Manzoni. (Corresponding author: Ning Wang.)

Lingfeng Shen is with the School of Information Engineering, Zhengzhou University, Zhengzhou 450001, China.

Ning Wang and Kon Max Wong are with the School of Information Engineering, Zhengzhou University, Zhengzhou 450001, China, and also with the Department of Electrical and Computer Engineering, McMaster University, Hamilton, ON L8S 4K1, Canada (e-mail: ienwang@zsu.edu.cn).

Di Zhang and Xiaomin Mu are with the School of Information Engineering, Zhengzhou University, Zhengzhou 450001, China.

Jun Chen is with the Department of Electrical and Computer Engineering, McMaster University, Hamilton, ON L8S 4K1, Canada.

Digital Object Identifier 10.1109/TGCN.2022.3186841

I. INTRODUCTION

MASSIVE machine-type communication (mMTC) is the core technology for the deployment of Internet of Things (IoT) in 5G scenarios, and as such, it has attracted significant research interests in recent years [1], [2]. Machine-type communication devices (MTCs) are known for their ability in processing information without human assistance. Efficient data acquisition, analysis and transmission are therefore major research topics for the mMTC technology. The 3rd Generation Partnership Project (3GPP) proposed a series of technical solutions to support mMTC services [3], [4]. However, achieving energy-efficient data collection for massive MTCs with scalable connectivity is still a challenging problem.

Due to their low-cost, small size and high mobility, unmanned aerial vehicles (UAVs) have recently been employed in many communication applications [5]–[8]. The 5G mMTC scenario is characterized by a large number and widely distributed MTCs [9], which requires more resources and infrastructure to support. Furthermore, these battery-powered devices need to transmit data with very low energy consumption to extend the operational lifetime. A moving UAV station can fly over every MTC to achieve highly energy-efficient data transmissions over the line-of-sight (LoS) communication links. This idea of UAV-aided data collection is advantageous over the conventional data collection techniques, and has become a promising data collection scheme for mMTC networks.

UAV-assisted data collection has been studied from the perspectives of optimal mission completion time and transmission rate. Jointly optimizing the UAV trajectory and sensors wake-up scheduling to minimize the maximum mission completion time was studied in [10]. Minimum mission time in emergency applications was studied in [11] by optimizing the UAV trajectory, altitude, velocity, and link scheduling. In [12], the system throughput of the UAV-aided simultaneous uplink and downlink transmission networks was maximized by optimizing the 3D UAV trajectory, communication scheduling, and transmission power between the UAV and sensor nodes. The UAV interference channel (UAV-IC) was investigated in [13] to address the strong cross-link interference challenge caused by the dominant LoS links. A joint trajectory and power

control problem for maximizing the aggregate sum-rate was formulated and solved subsequently.

However, it was noted that the UAVs and the MTCs are both energy-limited devices [14], [15]. Improving the transmission rate and minimizing the mission time under limited energy budget needs to be studied. To support delay-oriented IoT services, a computing task scheduling problem was studied in [16], where the task processing delay under the UAV energy capacity constraint was minimized. Extending the lifetime of UAVs and MTCs through wireless charging was investigated in [17], [18], which requires more resources and infrastructure, i.e., wireless chargers, to support. To overcome the drawbacks of limited UAV coverage and access capacity in a large supervised area, dividing the physical environment into multiple grids and collecting data is an effective way that shortens the link distance and preserves energy consumption [19]. Similarly, the idea of clustered service was proposed in [20]. However, jointly optimizing clustering and UAV deployment strategies is highly complex. Although significantly improves the data collection energy efficiency, the strategy proposed in [20] does not have any theoretical guarantee of the performance.

In this paper, we examine the design of efficient and scalable UAV-enabled data collection schemes for mMTC networks from an energy-aware perspective. The focus of this work is on the overall energy consumption of both the UAV and the MTCs. Given the data collection task, we formulate the problem of minimizing the energy consumption of the mMTC network. Three data-collection strategies, designated the Global Optimum (GOP), the Clustered Global Optimum (C-GOP) and the Clustered Particle Swarm Optimization (C-PSO), are proposed for different application scenarios. Specifically, the GOP strategy is developed for a small MTCs crowd distributed over a small area. Here, we show that whether the optimal trajectory can be found depends on the flying altitude of the UAV. On the other hand, based on the cluster strategy, we establish the C-GOP and C-PSO strategies to overcome the shortcomings of the GOP algorithm when the MTCs number or distribution area is large. This is carried out, respectively, by selecting for the UAV the MTCs within the *a priori* limited service radius to form its closest serving MTC set, and by locating the optimum UAV hovering point for each serving MTC set which, together with the UAV hovering position, are dynamically adjusted until all the MTCs are served. The effectiveness of the GOP, C-GOP and C-PSO algorithms under different circumstances are clearly verified using simulation examples.

II. SYSTEM MODEL AND PROBLEM FORMULATION

We consider an mMTC network which consists of M stationary MTCs. A vertical take off and landing (VTOL) UAV is used to collect data from the MTCs. A demonstration of the system model is shown in Fig. 1. In this work, we are going to maximize the energy efficiency of this UAV-enabled data collection system by optimizing the UAV's flying trajectory.

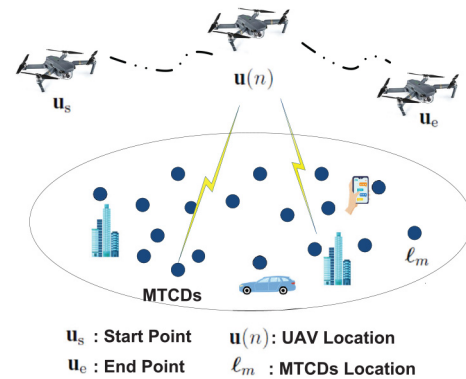


Fig. 1. The UAV-assisted data collection system model.

A. UAV-Assisted Data Collection System Model

Consider a set of MTCs \mathcal{D} consisting of M stationary MTCs which are distributed on a flat area of zero altitude. The locations of MTCs are fixed and are denoted as $\ell_m = (X_m, Y_m, 0)$, $m = 1, \dots, M$, where X_m and Y_m are the horizontal coordinates of the m^{th} MTC. The MTCs need to transmit data to a UAV. The UAV serves as a mobile data sink and flies on a 2D plane at a fixed altitude H , from a fixed start point to a predetermined end point within a finite time T , collecting data from the M MTCs on its way. Mathematically, whether the start and end points of the UAV trajectory are the same does not affect the algorithm design. To present and discuss the algorithm design in an intuitive way, we let the start and end points to be different points. We assume that the UAV flies at a constant velocity v . And in the first step, we further assume that positions of all MTCs are known to the system. Our task is to find an optimal flying trajectory for the UAV, which maximizes the overall energy efficiency of the system.

We denote the location of the start and end points of the UAV flight as $\mathbf{u}_s = (X_s, Y_s, H)$ and $\mathbf{u}_e = (X_e, Y_e, H)$, respectively. Let the total flight time T be divided into N equally distanced time instants t_0, t_1, \dots, t_N . Each time slot between two consecutive time instants is of duration $(t_n - t_{n-1}) = \Delta T_n = T/N$. The location of the UAV in-flight at the n^{th} time instant is $\mathbf{u}(n) = (x(n), y(n), H)$. We use $h_m(n)$, $m = 1, \dots, M$, $n = 0, 1, \dots, N$ to denote the wireless channel coefficient between the m^{th} MTC and the UAV at t_n . As in [22], $h_m(n)$ adopts the form

$$h_m(n) = \sqrt{\beta_m(n)}\gamma_m(n), \quad (1)$$

where $\beta_m(n)$ characterizes the large-scale effects such as path-loss and shadowing, $\gamma_m(n)$ is generally a complex-valued random variable with $\mathbb{E}[|\gamma_m(n)|^2] = 1$, which accounts for the small-scale fading. On the other hand, $\beta_m(n)$ takes different forms for Line of Sight (LoS) propagation and Non Line of Sight (NLoS) propagation, i.e.,

$$\beta_m(n) = \begin{cases} G_0/s_m^\alpha(n), & \text{LoS link} \\ \kappa G_0/s_m^\alpha(n), & \text{NLoS link} \end{cases} \quad (2)$$

where G_0 is the path-loss at the reference distance, α is the path loss exponent, $\kappa < 1$ reflects the additional attenuation

due to NLoS propagation, and s_m is the distance between the locations of m^{th} MTCD and the UAV at t_n . We note that:

$$s_m(n) = \sqrt{H^2 + (x(n) - X_m)^2 + (y(n) - Y_m)^2}. \quad (3)$$

At any time instance, either LoS or NLoS propagation occurs according to certain probabilistic model. In this work, we assume the probability of LoS propagation is given by

$$\Pr_L^m(n) = \frac{1}{1 + \varphi \exp(-\zeta[\theta_m(n) - \varphi])}, \quad (4)$$

where φ, ζ are parameters determined by the radio propagation environment, and $\theta_m(n) = \arcsin(\frac{H}{s_m(n)})$ is the elevation angle. The probability of NLoS propagation is $\Pr_{NL}^m(n) = 1 - \Pr_L^m(n)$.

B. Energy Consumption Model

The energy consumption of the system consists of two parts:

1) *Data Transmission Energy Consumption*: Each MTCD transmits its data to the UAV from its position ℓ_m at the appropriate n^{th} time slot. Thus, the total data transmission energy of the system is given by:

$$E_T = \sum_{m=1}^M \sum_{n=1}^N p_m(n) \cdot \Delta T_n \quad (5)$$

where $p_m(n)$ denotes the transmitting power consumption of the m^{th} MTCD during the n^{th} time slot and $\Delta T_n = \frac{T}{N}$ is the duration of the time slot. Here, we assume that each time slot is short enough such that the transmission power consumption of a MTCD device remains unchanged within the slot, but may change from slot to slot.

2) *UAV Maneuvering Energy Consumption*: We consider two kind of UAV maneuvers [23] that consumes energy in this system:

a) *Flying*: This is when the UAV is flying at a certain altitude. In our model, we assume the UAV to fly from start to end in N time slots. We also assume that within the n^{th} time slot, the velocity $v(n)$ of the UAV is maintained at a constant, so that the UAV energy consumption for flying is proportional to the distance covered [23]. Thus, the sum of the flying energy needed for the whole flight (all the time slots) is given by

$$E_{M_f} = \sum_{n=0}^N \frac{W_v g}{D \eta_m \eta_p} v(n) \cdot \Delta T_n, \quad (6)$$

where W_v, g, D, η_m and η_p represent respectively the mass of the UAV, the gravitational constant, the UAV's lift-drag ratio, the efficiency of the motor and propellers. Now, the start and end points of the UAV flight are $\mathbf{u}_s = (X_s, Y_s, H)$ and $\mathbf{u}_e = (X_e, Y_e, H)$, corresponding to the UAV flight time instants at t_0 and t_N respectively. Thus we can write $(X_s, Y_s, H) = (x(0), y(0), H)$ and $(X_e, Y_e, H) = (x(N), y(N), H)$. Noting that $v(n) \cdot \Delta T_n$ is the distance $r(n)$ travelled by the UAV during the n^{th} time slot, then the energy consumption of the flying UAV in Eq. (6) can be written as

$$E_{M_f} = \frac{W_v g}{D \eta_m \eta_p} \sum_{n=0}^N r(n), \quad (7)$$

where, for $n = 0, 1, \dots, N$,

$$r(n) = \sqrt{(x(n+1) - x(n))^2 + (y(n+1) - y(n))^2}. \quad (8)$$

b) *Hovering*: This is when the UAV is staying at a constant altitude from the ground maintaining at a stationary position. In this case, the energy consumption for UAV is directly proportional to the duration it hovers. Thus, if the UAV hovers at K spots during its total flight each time lasting τ_k seconds, then the total energy consumption for UAV hovering is given by [23]

$$E_{M_h} = \sqrt{\frac{(W_v g)^3}{2\pi \rho r_p^2 \nu_p}} \sum_{k=1}^K \tau_k, \quad (9)$$

where W_v, g and ρ are the mass of UAV, the gravitation constant, and the air density, r_p and ν_p denote respectively the radius and the number of the UAV's propellers, τ_k represents the duration of the UAV hovering at the k^{th} spot during its flight.

C. Data Transmission and Minimum Energy Consumption

The mission of the UAV is to collect the communication data from all MTCDs before the completion of its flight. The accomplishment of this mission is assured if the sum of achievable transmission rates of all time slots for each MTCD satisfies the following inequality.

$$\sum_{n=1}^N \mathbb{E} \left[B \log_2 \left(1 + \frac{p_m(n) |h_m(n)|^2}{\sigma^2} \right) \Delta T \right] \geq B_m, \quad (10)$$

$$m = 1, \dots, M,$$

where B denotes the communication bandwidth that is assigned to every MTCD. The left side of the inequality (10) represents the total reachable transmission rate of the m^{th} MTCD in the N time slots, B_m denotes the data size of the m^{th} MTCD needed to be transmitted and σ^2 denotes noise power which, for simplicity, is assumed to be constant for all the time slots of the flight. Equation (10) is difficult to handle when optimizing the UAV trajectory. To circumvent this, a lower bound is proposed to replace the left side of Eq. (10). Define $\lambda_m(n) = 1/\beta_m(n) |\gamma_m(n)|^2$, $\log_2(1 + \frac{p_m(n)}{\lambda_m(n) \sigma^2})$ is a convex function of $\lambda_m(n)$. A lower bound of the expected throughput can be derived according to Jensen's inequality as

$$\begin{aligned} & \mathbb{E} \left[B \log_2 \left(1 + \frac{p_m(n) |h_m(n)|^2}{\sigma^2} \right) \right] \\ & \geq B \log_2 \left(1 + \frac{p_m(n)}{\mathbb{E}[\lambda_m(n)] \sigma^2} \right) \\ & = B \log_2 \left(1 + \frac{p_m(n) (\Pr_L^m(n) + (1 - \Pr_L^m(n)) \kappa) G_0}{\sigma^2 s_m^\alpha(n)} \right) \\ & \triangleq B \log_2 \left(1 + \frac{p_m(n) \hat{h}_m(n)}{\sigma^2} \right), \end{aligned} \quad (11)$$

where

$$\hat{h}_m(n) = \frac{(\Pr_L^m(n) + (1 - \Pr_L^m(n)) \kappa) G_0}{s_m^\alpha(n)}. \quad (12)$$

From Eq. (11), we can estimate the power utilized by an MTCD for the transmission of data: The arithmetic average rate of data transmission of the m^{th} MTCD can be written as

$$\begin{aligned}\bar{\rho}_m &= \frac{1}{N} \sum_{n=1}^N B \log_2 \left[1 + \frac{p_m(n) \hat{h}_m(n)}{\sigma^2} \right] \\ &= B \log_2 \left[1 + \frac{p_m(n) \hat{h}_m(n)}{\sigma^2} \right],\end{aligned}\quad (13)$$

where $\left[1 + \frac{p_m(n) \hat{h}_m(n)}{\sigma^2} \right] = \left[\prod_{n=1}^N \left(1 + \frac{p_m(n) \hat{h}_m(n)}{\sigma^2} \right) \right]^{1/N}$ is the geometric mean of $\left\{ 1 + \frac{p_m(n) \hat{h}_m(n)}{\sigma^2} \right\}, n = 1, \dots, N$. Now, writing \bar{h}_m as the mean channel response for the m^{th} MTCD over the whole flight of the UAV, we can write

$$\bar{\rho}_m = B \log_2 \left[1 + \frac{p_m(n) \hat{h}_m(n)}{\sigma^2} \right] \approx B \log_2 \left[1 + \frac{\bar{p}_m \bar{h}_m}{\sigma^2} \right],$$

where \bar{p}_m denotes the estimate of the m^{th} MTCD transmission power. From Eqs. (10) and (13), we have $\sum \bar{\rho}_m \cdot \Delta T = \bar{\rho}_m T = B_m$, we can thus write

$$\bar{p}_m \approx \left(2^{\frac{B_m}{BT}} - 1 \right) \sigma^2 / \bar{h}_m. \quad (14)$$

For completion of the data collection task from the MTCDs, it is also desirable to design a flight trajectory for the UAV involving the least energy consumption. By so doing, we allow the two parts of energy consumption, i.e., the data transmission energy and the UAV manoeuvring energy, to take on different weights, reflecting the different emphasis of needs in the system. In the subsequent sections, based on the mission of completing the task of data transmission while minimizing system energy consumption, we will apply two strategies to design different trajectories for the UAV for collecting data from the MTCDs.

III. THE GOP NON-STOP OPTIMAL TRAJECTORY DESIGN

We first consider the planning of a flight trajectory for which the UAV completes its flight within a stipulated time T_y while collecting data from all MTCDs. During the flight, the UAV does not hover at any point but may fly at different velocities within the N different segments of T . Based on this strategy, the corresponding optimization problem can be formulated as,

$$\begin{aligned}\mathbf{P0}: \quad & \text{minimize} && w_1 E_T + w_2 E_{M_f} \\ & \{x(n), y(n), p_m(n)\}_{n=1}^N \\ \text{s.t.} \quad & \text{for } m = 1, \dots, M, \quad n = 1, \dots, N \\ & \text{(i)} \quad 0 \leq p_m(n) \leq p_{max} \\ & \text{(ii)} \quad \sum_{n=1}^N B \log_2 \left(1 + \frac{p_m(n) \hat{h}_m(n)}{\sigma^2} \right) \geq B_m, \\ & \text{(iii)} \quad 0 < [x(n) - x(n-1)]^2 + [y(n) - y(n-1)]^2 \\ & \leq [v_{max} \cdot \Delta T_n]^2\end{aligned}\quad (15)$$

where p_{max} is the maximum power of MTCDs. Based on the energy consumption model of the GOP strategy, absolute hovering state is not considered. Denote by v_{max} the maximum flying speed of the UAV, the corresponding mobility constraint

is therefore $0 < [x(n) - x(n-1)]^2 + [y(n) - y(n-1)]^2 \leq [v_{max} \cdot \Delta T_n]^2$. Let us now examine the optimization problem **P0** in (17).

A. Discussion on the Convexity

Objective Function: The energy consumption terms are weighted respectively by w_1 and w_2 reflecting on our emphasis on the importance of the two types of energy. Here, we stipulate that $w_1 + w_2 = 1$. As shown in Eq. (5), E_T is a linear function of $p_m(n)$. On the other hand, E_{M_f} , as shown in Eq. (7), can also be shown to be convex since, writing Eq. (8) as $r(n) = \sqrt{(\Delta x)^2 + (\Delta y)^2}$, we have

$$\begin{aligned}\frac{\partial^2 r(n)}{\partial \Delta x^2} &= \frac{(\Delta y)^2}{\left[(\Delta x)^2 + (\Delta y)^2 \right]^{\frac{3}{2}}}, \\ \frac{\partial^2 r(n)}{\partial \Delta y^2} &= \frac{(\Delta x)^2}{\left[(\Delta x)^2 + (\Delta y)^2 \right]^{\frac{3}{2}}},\end{aligned}$$

and

$$\frac{\partial^2 r(n)}{\partial \Delta x \partial \Delta y} = \frac{\partial^2 r(n)}{\partial \Delta y \partial \Delta x} = \frac{\Delta x \Delta y}{\left[(\Delta x)^2 + (\Delta y)^2 \right]^{\frac{3}{2}}}.$$

The Hessian matrix of $r(n)$ is therefore

$$\nabla^2 r(n) = \begin{bmatrix} \frac{\Delta y^2}{\left[(\Delta x)^2 + (\Delta y)^2 \right]^{\frac{3}{2}}} & \frac{\Delta x \Delta y}{\left[(\Delta x)^2 + (\Delta y)^2 \right]^{\frac{3}{2}}} \\ \frac{\Delta x \Delta y}{\left[(\Delta x)^2 + (\Delta y)^2 \right]^{\frac{3}{2}}} & \frac{\Delta x^2}{\left[(\Delta x)^2 + (\Delta y)^2 \right]^{\frac{3}{2}}} \end{bmatrix}.$$

For any $\mathbf{z}^T(n) = [z_1(n) \quad z_2(n)]$,

$$\mathbf{z}^T(n) \left[\nabla^2 r(n) \right] \mathbf{z}(n) = \frac{[z_1(n) \Delta y + z_2(n) \Delta x]^2}{\left[(\Delta x)^2 + (\Delta y)^2 \right]^{\frac{3}{2}}} \geq 0. \quad (16)$$

Therefore, $\nabla^2 r(n)$ is positive semi-definite, which verifies convexity of the objective function [24].

Constraints: First, the mobility constraint is non-convex, which can be relaxed by dropping the left inequality to have convexity. As a result, we have a convex mobility constraint in problem **P1**, which is $[x(n) - x(n-1)]^2 + [y(n) - y(n-1)]^2 \leq [v_{max} \cdot \Delta T_n]^2$. The problem (15) is therefore transformed as

$$\begin{aligned}\mathbf{P1}: \quad & \text{minimize} && w_1 E_T + w_2 E_{M_f} \\ & \{x(n), y(n), p_m(n)\}_{n=1}^N \\ & \text{s.t. for } m = 1, \dots, M, \quad n = 1, \dots, N \\ & \text{(i)} \quad 0 \leq p_m(n) \leq p_{max} \\ & \text{(ii)} \quad \sum_{n=1}^N B \log_2 \left(1 + \frac{p_m(n) \hat{h}_m(n)}{\sigma^2} \right) \geq B_m, \\ & \text{(iii)} \quad [x(n) - x(n-1)]^2 + [y(n) - y(n-1)]^2 \\ & \leq [v_{max} \cdot \Delta T_n]^2\end{aligned}\quad (17)$$

It is worth noting that in the numerical studies in Section V, $[x(n) - x(n-1)]^2 + [y(n) - y(n-1)]^2$ approaching 0 has never been observed. In any GOP trajectory simulated, the UAV would slow down when flying over an MTCD cluster but the UAV speed is never negligibly small. Therefore, the

relaxation of constraint (iii) does not affect the optimality of the GOP strategy. Constraints (i) and (iii) are respectively linear and quadratic, and hence the convexity of problem **P1** depends on the convexity (concavity) of Constraint (ii).

B. Condition for a Globally Optimal Trajectory

We now states the condition for the convexity/concavity of Constraint (ii) in the following:

Lemma 1: Define r_{\max} as the maximum possible serving radius of the UAV in the data collection process, i.e.,

$$r_{\max} = \max \left\{ \sqrt{(x(n) - X_m)^2 + (y(n) - Y_m)^2} \right\},$$

$$m = 1, \dots, M, \quad n = 1, \dots, N.$$

Then the UAV in the problem of (17) can find a globally optimal trajectory if the flying altitude of the UAV $H \geq \sqrt{3}r_{\max}$.

Proof: Consider the term inside the brackets of Constraint (ii) in Eqs. (17). Obviously, When xy is a large number, $\log(1+x) \approx \log(x)$. Therefore,

$$\begin{aligned} & \log_2 \left(1 + \frac{p_m(n)(\Pr_L^m(n) + (1 - \Pr_L^m(n))\kappa)G_0}{\sigma^2 [H^2 + (x(n) - X_m)^2 + (y(n) - Y_m)^2]^{\frac{\alpha}{2}}} \right) \\ & \approx \log_2 \left(\frac{p_m(n)(\Pr_L^m(n) + (1 - \Pr_L^m(n))\kappa)G_0}{\sigma^2 [H^2 + (x(n) - X_m)^2 + (y(n) - Y_m)^2]^{\frac{\alpha}{2}}} \right) \\ & = \frac{\alpha}{2} \log_2 \left(\frac{c_m(n)}{H^2 + (x(n) - X_m)^2 + (y(n) - Y_m)^2} \right), \end{aligned} \quad (18)$$

where $c_m(n) = \left[\frac{p_m(n)(\Pr_L^m(n) + (1 - \Pr_L^m(n))\kappa)G_0}{\sigma^2} \right]^{\frac{2}{\alpha}}$. Let

$$q_m(n) = \frac{c_m(n)}{H^2 + (x(n) - X_m)^2 + (y(n) - Y_m)^2}. \quad (19)$$

We note that if $q_m(n)$ is concave and positive, then $\log(q_m(n))$ is concave. Now, it is assumed in Section II-B that the data transmission power consumption for a MTCN remains constant during each time segment ΔT_n . Assuming that $\Pr_L^m(n)$ does not change when optimizing the UAV's flying trajectory, $c_m(n)$ could be considered as a constant. Taking the second partial derivative of $q_m(n)$ with respect to $x(n)$ and $y(n)$, we obtain

$$\frac{\partial^2 q_m(n)}{\partial x^2(n)} = \frac{2c_m(n) [4(x(n) - X_m)^2 - s_m^2(n)]}{s_m^6(n)}, \quad (20a)$$

$$\frac{\partial^2 q_m(n)}{\partial y^2(n)} = \frac{2c_m(n) [4(y(n) - Y_m)^2 - s_m^2(n)]}{s_m^6(n)}, \quad (20b)$$

$$\frac{\partial^2 q_m(n)}{\partial x(n)\partial y(n)} = \frac{8c_m(n)(x(n) - X_m)(y(n) - Y_m)}{s_m^6(n)}. \quad (20c)$$

The Hessian matrix of $q_m(n)$ can now be written as

$$\nabla^2 q_m(n) = \begin{bmatrix} \frac{\partial^2 q_m(n)}{\partial x^2(n)} & \frac{\partial^2 q_m(n)}{\partial x(n)\partial y(n)} \\ \frac{\partial^2 q_m(n)}{\partial y(n)\partial x(n)} & \frac{\partial^2 q_m(n)}{\partial y^2(n)} \end{bmatrix}. \quad (21)$$

The concavity of Constraint (ii) of Eq. (17) is ensured [24] if:

a) both $\frac{\partial^2 q_m(n)}{\partial x^2(n)}$ and $\frac{\partial^2 q_m(n)}{\partial y^2(n)}$ are non-positive definite, and

b) $\det(\nabla^2 q_m(n)) \leq 0$.

Condition a) gives,

$$\begin{aligned} 4(x(n) - X_m)^2 - s_m^2(n) &\leq 0; \\ 4(y(n) - Y_m)^2 - s_m^2(n) &\leq 0. \end{aligned}$$

Substituting the value of $s_m(n)$ from Eq. (3) into the above two equations and adding, we have

$$H^2 \geq (x(n) - X_m)^2 + (y(n) - Y_m)^2. \quad (22)$$

Also, putting Eq. (3) into Condition b) and simplifying yields

$$H^2 \geq 3 \left[(x(n) - X_m)^2 + (y(n) - Y_m)^2 \right]. \quad (23)$$

Clearly, if (23) is satisfied, then (22) is satisfied. Furthermore, since concavity should be valid throughout the entire flight, H^2 should be larger than or equal to the maximum value of the righthand side of (23), i.e.,

$$H \geq \sqrt{3}r_{\max}. \quad (24)$$

Equation (24) guarantees the concavity of Constraint (ii), and thus the globally optimum solution can be found for the problem of Eq. (17). It is worth noting that $H \geq \sqrt{3}r_{\max}$ means that the elevation angle is greater than 60 degrees. According to [26], the occurrence probability of LoS is approximately equal to 1 when the elevation angle is greater than 60 degrees even in an urban environment. In this cases, the air-to-ground links can be viewed as LoS links. Therefore, when solving the optimal trajectory of the UAV, LoS occurrence probability parameters φ and ζ do not affect the restriction on the UAV flying height, thus the assumption that $\Pr_L^m(n)$ is constant at the beginning of this proof is reasonable. The optimal solution to **P0** is a global optimal trajectory in this case. ■

We designate the minimum UAV flying altitude indicated by Eq. (24) the *critical altitude*, and the optimum flight path obtained under the convexity condition the *GOP trajectory*.

C. Computational Complexity of the GOP Algorithm

The complexity of an algorithm largely depends on the scale (number of operational parameters) of the problem. For the GOP algorithm described above, establishing an N -step trajectory involves all the $M \times N$ transmission power variables $p_m(n)$, as well as the $2N$ co-ordinate variables of the trajectory anchor points. The total number of operational parameters for GOP is thus $\nu_0 = N(M + 2)$. Also, for the GOP algorithm, the number of constraints in the problem is another important factor. Here, we can see that the number of constraints is $\kappa_0 = 2MN + M + N$.

Now, if we use a gradient method (say, Newton's method) to solve the convex optimization problem, for each step of decent, we have to find the product $\mathbf{H}^{-1}\mathbf{g}$, where \mathbf{H} is a $\nu_0 \times \nu_0$ Hessian matrix, and \mathbf{g} is a $\nu_0 \times 1$ vector. The complexity of this process is $O(\kappa_0\nu_0^2)$. Furthermore, the number of iterations of Newton steps grows as $\sqrt{\kappa_0}$ [24].

From the above review of complexity, it can be concluded that if the number of MTCs and the number of trajectory anchor points are large, the complexity of the GOP algorithm may be prohibitive for a real-time optimization. Also, the UAV flying altitude H may have to be substantially large to guarantee convexity. This results in very large path-loss for data communications with the MTCs, putting an excessive demand on their transmission power. Hence, the GOP trajectory design should be mainly suitable for data collection scenarios where both the number of MTCs and the UAV service area are small.

IV. DYNAMIC TRAJECTORY DESIGN BASED ON MTC CLUSTERING

It can be seen from the above section that the implementation of a convex GOP algorithm requires large UAV flying altitude, which should be greater than $\sqrt{3}r_{max}$. As a result, when the task area of the UAV is large, the performance of the GOP algorithm deteriorates significantly. Also, the complexity of the GOP algorithm is positively correlated with the number of MTCs and the UAV's service time. Therefore, it can be seen that the GOP algorithm is not suitable for scenarios having large task areas, large number of MTCs, and long service durations. To overcome the difficulties arising from the GOP strategy, we consider clustered service strategies for data collection from the mMTC network. The UAV station travels across the clusters and collects data from each cluster while hovering above it. The problem then breaks down to the in-cluster hovering point optimization.

Let us first analyze the optimal hovering point in a UAV cluster. When the UAV is hovering, the energy consumption per second is constant, so the optimal hovering point that maximizes the energy efficiency is the hovering point that maximizes the achievable transmission rate. Assuming that there are M' MTCs in the cluster, the objective function for solving the optimal hover point can be described as $\sum_{m'=1}^{M'} B \log_2(1 + \frac{p'_m(\text{Pr}_L^{m'} + (1 - \text{Pr}_L^{m'})\kappa)G_0}{\sigma^2 s_m'^2})$. Let $c_{m'} = \frac{p'_m(\text{Pr}_L^{m'} + (1 - \text{Pr}_L^{m'})\kappa)G_0}{\sigma^2}$, writing $q_{m'} = (1 + \frac{c_{m'}}{s_m'^2})$, the objective function of can be rewritten as

$$\sum_{m'=1}^{M'} \log q_{m'} = \log \prod_{m'=1}^{M'} q_{m'}. \quad (25)$$

Since the UAV is always flying at the critical altitude, and since $\max q_{m'} \Rightarrow \max \log q_{m'}$, an optimum hovering position of the UAV can always be located. Let this optimum hovering position be denoted as (x^*, y^*, H) . The values of (x^*, y^*) thus satisfy

$$\frac{\partial}{\partial x} \left[\prod_{m'=1}^{M'} q_{m'} \right]_{x=x^*} = 0, \quad \frac{\partial}{\partial y} \left[\prod_{m'=1}^{M'} q_{m'} \right]_{y=y^*} = 0. \quad (26)$$

Carrying out the derivatives in (26) with respect to xy and y and equating to zero for maximum, we find the optimum

coordinates x^* and y^* satisfy the following condition:

$$x^* = \frac{\sum_{i=1}^{M'} a_i(x^*, y^*) X_i}{A(x^*, y^*)}, \quad y^* = \frac{\sum_{i=1}^{M'} a_i(x^*, y^*) Y_i}{A(x^*, y^*)}, \quad (27)$$

where $a_i(x^*, y^*) = s_i^{-2}(x^*, y^*) [\prod_{m'=1, m' \neq i}^{M'} q_{m'}(x^*, y^*)]$ and $A(x^*, y^*) = \sum_{i=1}^{M'} a_i(x^*, y^*)$, with s_i^2 being given by Eq. (3). Thus, for any distribution of the M' MTCs, we can see from Eq. (27), the optimum hovering planar coordinates (x^*, y^*) are the *weighted mean* of the M' coordinates of the MTCs, each with weighting coefficient a_i/A , where a_i and A both are functions of x^* and y^* .

To cluster MTCs and solve x^* , y^* , we propose two clustering-based data collection algorithms in the following.

A. The C-GOP and C-PSO Trajectory Design Algorithms

1) *The C-GOP Design*: From Lemma 1, we observe that if the UAV's instantaneous serving area is confined to a relatively smaller size, the required flying altitude for finding an optimal trajectory will then be lower, and the channel condition will improve accordingly. Thus, we can first fix the UAV flight altitude H , and obtain the corresponding maximum UAV service radius $r_{max} \leq H/\sqrt{3}$ for a sub-group of MTCs. We also allow the UAV to hover at K_y different spots during its flight to collect data from each of these sub-groups of MTCs. This means that the limit on the total UAV flight time T has to be relaxed. At the k^{th} hovering spot, let the UAV's service radius be $r_k \leq r_{max}$, and let there be M'_k MTCs to be serviced. We also limit the number of MTCs being serviced at any time such that $M'_k \leq M'_{max}$ with M'_{max} being the assigned maximum capacity of the service area covered by r_{max} . The UAV will stay hovering at the k^{th} spot collecting data until all the MTCs within the service radius r_k have completed transmission. At that point, the UAV will choose another set of MTCs and select the $(k+1)^{\text{th}}$ optimal hovering spot. During the UAV transition from the k^{th} to the $(k+1)^{\text{th}}$ hovering point, there is no data transmission from the MTCs and the hovering and flying altitude of the UAV is kept at $H \geq \sqrt{3}r_{max}$.

We denote the duration of the UAV hovering at the k^{th} spot τ_k . Let the positions of the UAV and the m^{th} MTCs being serviced during the k^{th} hovering time be $[x_k, y_k, H]$ and $[X_{m'}(k), Y_{m'}(k), 0]$; $m' = 1, \dots, M'_k$ respectively. It is desired that the points at which the UAV hovers are chosen to minimize the system energy expenditure. Let us examine each of these energy items from the view point of the present strategy.

a) *Data transmission energy and UAV hovering energy*: If the time that the UAV spent hovering at the k^{th} spot is τ_k , meanwhile data are transmitted from the M'_k MTCs covered within the service radius, then from Eqs. (5) and (9), the energy for data transmission and for UAV hovering during the k^{th} hovering period can be respectively written as

$$E_T(k) = \sum_{m'=1}^{M'_k} p_{m'} \tau_k, \quad (28a)$$

$$E_{M_h}(k) = \sqrt{\frac{(W_v g)^3}{2\pi \rho r_p^2 \nu_p}} \tau_k, \quad (28b)$$

where $p_{m'}$, the power used by the m^{th} MTCD for data transmission, is assumed to be equal for all users. To minimize the two energy consumptions, we must minimize the hovering time τ_k . However, τ_k represents the time taken by the fastest MTCD to transmit all its data, and is unknown in general. Thus, we will treat τ_k as a random variable and attempt to minimize its expected value $E[\tau_k]$. The average data transmission time is inversely proportional to the average channel capacity, which, from Eqs. (11) and (12), for the hovering period τ_k , can be written as

$$\bar{C}_k = \frac{1}{M'} \sum_{m'=1}^{M'} B \log \left(1 + \frac{p_{m'} \hat{h}_{m'}(k)}{\sigma^2} \right), \quad (29)$$

where $s_{m'}^2(k)$ given by Eq. (3), is the squared distance between the m^{th} MTCD and the UAV. Thus, our objective is to design a flight path on which the k^{th} hovering position of the UAV maximizes \bar{C}_k of Eq. (29).

b) Flight path: The flight path is immediately fixed once the hovering points are determined. Thus the energy consumption for flying is dependent only on the positions of the hovering points. The flight path of the UAV is then obtained by the straight lines joining one by one the optimum hovering points. The different optimum spots at which the UAV hovers are determined by solving the following optimization problem:

$$\begin{aligned} \mathbf{P2}: \quad & \text{maximize}_{\{x_k, y_k\}} \sum_{m'=1}^{M'} B \log \left(1 + \frac{p_{m'} \hat{h}_{m'}(k)}{\sigma^2} \right) \\ \text{s.t.} \quad & \text{(i) } M' \leq M'_{\max} \\ & \text{(ii) } (x_k - X_{m'}(k))^2 + (y_k - Y_{m'}(k))^2 \leq r_{\max}^2 \quad (30) \end{aligned}$$

By inspecting Eq. (30), it can be shown that the two mild constraints are readily satisfied. Also, as shown in Lemma 1, as long as the UAV is flying at, or above, the critical altitude, the objective function in **P2** is concave and an optimum hovering spot (x_k^*, y_k^*, H) can be located. Thus, the present strategy instructs the UAV to keep its flying altitude at $H \geq \sqrt{3} r_{\max}$, locate its first service set of M'_1 MTCDs, maneuver to the optimal hovering point (x_1^*, y_1^*) for the service set by solving Problem **P2** and starts collecting data from the MTCDs. When one MTCD finishes its transmission task, it is dropped out of the UAV's service set. Another MTCD having the best channel condition within the UAV's service radius is then selected to enter the service set. If the UAV has served all MTCDs within the current service radius and there is no other MTCDs to join its service set, it then flies straight to the nearest MTCD location outside the current service radius and updates the service set. Meanwhile, Problem **P2** needs to be updated and solved again, which gives the new optimal hovering location of the UAV. This process repeats until all MTCDs are served and the UAV will then fly to its ending location. The algorithm is designated C-GOP and is summarized in Algorithm 1.

2) *The C-PSO Design:* While the C-GOP can reduce the UAV flying altitude by clustering the ground-based MTCDs, having a relatively large service radius r_{\max} may still result

Algorithm 1 The Greedy Dynamic Trajectory Design

Input: MTCD set \mathcal{D} , the UAV flying altitude H , the radius of the serving region r_{\max} , the UAV service capacity M'_{\max} , the effective channel power gain G_0 , the transmission power p_m and the AWGN variance σ^2 .

Output: UAV K_y optimal hovering positions $(x^*(k), y^*(k))$ on its flight.

- 1: Initialization: The UAV current location (x_k, y_k) , $k=1$.
 - 2: **while** \mathcal{D} is not a empty set **do**
 - 3: Let the MTCDs set served by the UAV at this location is $\mathcal{D}' = \emptyset$ and the number of MTCDs in \mathcal{D}' as $M' = 0$.
 - 4: **for** every MTCD $m \in \mathcal{D}$ **do**
 - 5: Calculate the distance between the UAV current location and the m^{th} MTCD as $d_m^2 = (x_k - X_m)^2 + (y_k - Y_m)^2$, $\Omega = \{d_m, m \in \mathcal{D}\}$
 - 6: **end for**
 - 7: $m^* = \arg \min \Omega$
 - 8: **if** $\min\{\Omega\} > r_0$ **then**
 - 9: Let $x_k = X_{m^*}, y_k = Y_{m^*}$, go back to step 4.
 - 10: **else**
 - 11: **while** $\min\{\Omega\} \leq r_0$ **do**
 - 12: **if** $M' \leq M'_{\max}$ **then**
 - 13: move m^{th} MTCD from set \mathcal{D} to set \mathcal{D}' , change $d_m^* = +\infty, M' = M' + 1$.
 - 14: **else**
 - 15: break
 - 16: **end if**
 - 17: **end while**
 - 18: Solve P2 with MTCDs set \mathcal{D}' and put the result (x_k^*, y_k^*) in (x_k^*, y_k^*) .
 - 19: Let $x_k = x_k^*, y_k = y_k^*, k = k + 1$.
 - 20: **end if**
 - 21: **end while**
 - 22: All hover positions (x_k^*, y_k^*) are obtained, which constitute the UAV's dynamic trajectory.
-

in a large flying altitude of the UAV, which inevitably causes greater maneuvering energy consumption and delay. To overcome this issue, the idea of Particle Swarm Optimization can be employed. By mimicking the foraging behavior of birds, the PSO algorithm designs a simple mechanism to guide particles to search for the optimal solution. Examining **P2**, we observe that locating the optimal hovering point within the service radius of a UAV is similar to that of birds searching for food. Therefore, the idea and the algorithm of the PSO can be applied to the problem under investigation as follows:

Suppose there are L points in the two-dimensional space determined by the UAV's service radius. Each point represents a feasible hovering position $P_\ell = (x_\ell, y_\ell)$ for the UAV, and each is occupied by a particle having a velocity $v_\ell = (v_{x_\ell}, v_{y_\ell})$. Each position is associated with a fitness value f_ℓ , corresponding to the particle's motion strategy and the value of the UAV hovering at that position. Here, the fitness value is defined by the objective function of **P2**, and it determines the optimal position of each particle with respect

to the group being searched. Let the optimal solutions sought after by the ℓ^{th} particle and by the group be S_ℓ and S_L , respectively. Then, the strategy for governing the motion of the ℓ^{th} particle can be written as

$$v_\ell^{(k+1)} = wv_\ell^{(k)} + c_1r_1\left(S_\ell^{(k)} - P_\ell^{(k)}\right) + c_2r_2\left(S_L^{(k)} - P_\ell^{(k)}\right), \quad (31)$$

where $\cdot^{(k)}$ denotes the number of iterations, w is the inertia weighting representing the continuation of the particle's previous motion state, c_1, c_2 are factors that improve particle's search state by learning the optimal historical position, r_1, r_2 are random numbers in the interval $(0, 1)$ enhancing the random search of particle's position. The particle position can be updated such that

$$P_\ell^{(k+1)} = P_\ell^{(k)} + v_\ell^{(k+1)} \cdot \tau_u, \quad (32)$$

where τ_u is a time step. The velocities and positions of the particles are updated until the fitness value's change with iteration is less than a pre-set threshold, or a predefined maximum number of iterations is reached. The threshold is usually the acceptable small error in numerical simulations, e.g., 10^{-6} . The update strategy of the particle velocity in Eq. (22) ensures that the particles continue to search for the optimal solution as the number of iterations increases. When the particle reaches the optimal solution, $S_\ell = S_L$, the particle oscillates in the neighborhood of the optimal solution with radius $wv_\ell^{(k)}$ until the stopping condition of the algorithm is met.

The PSO algorithm does not require the problem to be convex, hence the limitation of UAV altitude in our problem can be circumvented. The drawback is that the hovering points obtained by PSO algorithm have no optimality guarantee.

B. Computational Complexity of the C-GOP and C-PSO Algorithms

Evaluation of the complexity of C-GOP algorithm is similar to that of the GOP strategy. Here, the number of variable parameters is simply the co-ordinates of each hovering point (x_k, y_k) , i.e., $\nu_R = 2$. From each hovering point, the C-GOP algorithm calculates the co-ordinates of the next hovering point by solving a convex optimization problem using a gradient-based method. Similar in steps to the analysis of the GOP algorithm, we find the scale of the C-GOP to be $\nu_R = 2$, and the number of constraints $\kappa_R = M + 1$. Hence the complexity of the algorithm is $O(\kappa_R \nu_R^2)$, which is much lower than that of the GOP. This is because the GOP strategy requires the entire optimum flight path to be calculated based on global knowledge of the system, whereas in the C-GOP, only local optimization is performed from one point to the next.

Unlike GOP and C-GOP, the complexity of the C-PSO algorithm only depends on the number of particles and the number of iterations, regardless the number of optimization variables and constraints [25]. Therefore, the complexity of C-PSO is not affected by the size of the problem. In the simulations, the number of particles and the maximum iteration times are fixed parameters, and these two parameters determine the upper bound of the complexity of the particle swarm algorithm.

TABLE I
PARAMETER VALUES OF THE SYSTEM SETTING FOR SIMULATIONS

Parameter	Value	Parameter	Value	Parameter	Value
v_{max}	15 m/s	σ^2	-174 dBm/H	B	10 kHz
m	1.5 kg	r_p	30 cm	D	13 cm
n_p	4	η_m	0.94	η_p	0.85
φ	9.6	G_0	45 dB	κ	0.2
ζ	0.28	B_m	24 Mbits	-	-

V. SIMULATION RESULTS AND DISCUSSION

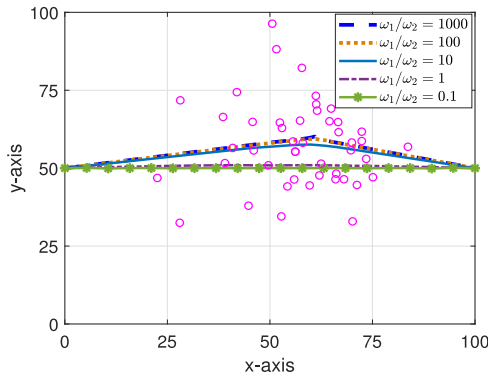
In this section, numerical studies of UAV flight trajectory design are conducted using the algorithms investigated in previous sections. Simulations of the optimized trajectories for the UAV collecting data from MTCs are also presented. Performance comparison with existing state-of-the-art work dealing with similar scenarios is conducted. The parameter values of the UAV and the communication environment are summarized in Table I.

The flight trajectory designs and the data collection performance of the UAV are examined. In all the examples, we assume that the MTCs are Gaussian distributed physically in a square area called the *task area*, the starting and the ending points of the UAV flights are respectively fixed at $[0, a/2]$ and $[a, a/2]$, where a is the side length of the task area. Activities of the UAV under different scenarios are simulated in this task area. Discussions and inferences are drawn from the observed trajectories and their performance under different parameter values.

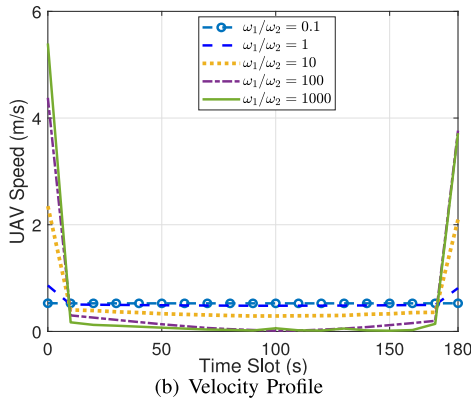
A. Trajectories and Data Collection Performance of GOP

(i) Here, the total UAV flight time is set to $T = 180$ seconds, and each time slot $\Delta T_n = 1.0$ second. The side length of the task area is set to $a = 100$ m. The MTCs are Gaussian distributed in the two dimensional space. The mean of the position coordinates are $\bar{X} = 60\text{m}$, $\bar{Y} = 60\text{m}$, and the corresponding variances are $\sigma_x^2 = \sigma_y^2 = 25$. The value of r_{max} for the GOP strategy is designated as the distance to the MTCD farthest away from the UAV starting point.

Fig. 2(a) shows the distribution of the MTCs (small red circles) in the area and the GOP trajectories designed with different weighting ratios w_1/w_2 . It can be observed that all the trajectories lead the UAV flying from the start point to the end point, passing through the cluster of MTCs. The larger relative weight is assigned to the transmission energy consumption in the objective function, the closer the UAV is directed into the MTCD cluster center. Conversely, when larger relative weight is assigned to the UAV maneuvering energy consumption, the flying trajectory tends to go along a straight line from the start point to the end point. Fig. 2(b) shows the UAV velocity profile for different values of weighting ratios w_1/w_2 . It can be observed that, for all cases with different w_1/w_2 values, the UAV always slows down to a steady speed when it passes the MTCD cluster. The larger relative weight is assigned to the transmission energy consumption, the larger UAV velocity drop is observed. Both Figs. 2(a) and 2(b) show that the more emphasis is put on data transmission energy

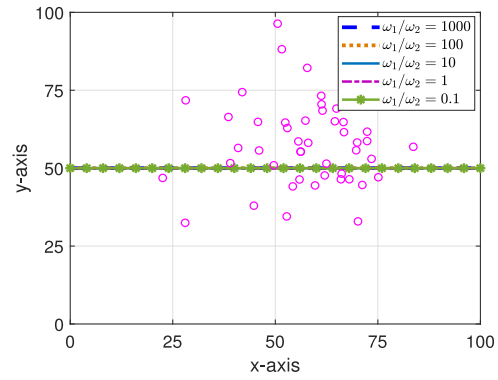


(a) Designed Trajectories

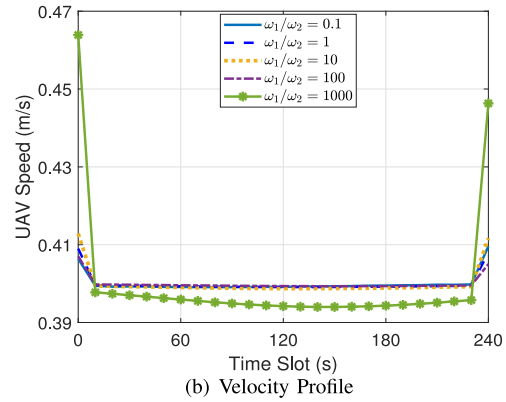


(b) Velocity Profile

Fig. 2. GOP trajectory design at different w_1/w_2 for collecting data from a Gaussian distributed MTCD crowd $N(60, 60, 25, 25)$, $T = 180$ sec, $M = 50$.



(a) Designed Trajectories



(b) Velocity Profile

Fig. 3. GOP trajectory design at different w_1/w_2 for collecting data from a Gaussian distributed MTCD crowd $N(60, 60, 25, 25)$, $T = 240$ sec, $M = 50$.

consumption, the deeper the UAV flies into the user cluster and the slower it traverses through the cluster.

(ii) We extend the flight time to 240 seconds while the other parameters are kept the same as in the simulations above.

From Fig. 3(a) we observe that as the flight time is extended, the optimum trajectories all approach a straight line going directly from the start point to the end point. Similar to Fig. 2(b), in Fig. 3(b) it is shown that the UAV slows down to a steady speed when it passes the MTCD cluster for data collection with all weighting ratio values.

Fig. 4 shows different energy consumptions of the UAV based on the GOP strategy. Fig. 4(a) presents the total data transmission energy consumption for different overall mission time T , i.e., $2E_T = 2M \times \bar{e}_m$ where e_m is the value of average data transmission energy per MTCD for each of the flights, and $\bar{e}_m = \frac{1}{M} \sum_{m=1}^M \sum_{n=1}^N p_m(n) \cdot \Delta T_n$. $p_m(n)$ is the optimized transmit power of the m^{th} MTCD during the n^{th} time slot. $\Delta T_n = \frac{T}{N}$ is the duration of the n^{th} time slot. Here, a factor 2 is present because the receiver energy consumption by the UAV is assumed to be the same as that for data transmission by the MTCDs. It can be observed in Fig. 4(a) that with the extension of the flight time, the data transmission energy is reduced dramatically. This can be explained by examining the estimate of the average transmission power for the m^{th} MTCD in Eq. (14). For example, substituting the data size $B_m = 24$ Mbits as well as the flight times to be $T_1 = 150$ seconds and $T_2 = 180$ seconds, we

find

$$\frac{\hat{p}_{T_1}}{\hat{p}_{T_2}} = \frac{2 \frac{B_m}{BT_1} - 1}{2 \frac{B_m}{BT_2} - 1} \approx 2 \left(\frac{B_m}{BT_1} - \frac{B_m}{BT_2} \right) = 2^{2.67} \approx 6.36.$$

This yields the data transmission energy ratio of the two cases to be

$$\frac{E_{T_1}}{E_{T_2}} = \frac{\bar{e}_{T_1}}{\bar{e}_{T_2}} = \frac{\hat{p}_{T_1} \times T_1}{\hat{p}_{T_2} \times T_2} \approx 5.3. \quad (33)$$

Comparing the data transmission energy consumption shown in Fig. 4(a), the above ratios agree well with the plot. Another observation is that the data transmission energy decreases slightly as the transmission energy consumption is more emphasized, i.e., w_1/w_2 increases. Fig. 4(b) shows the flying energy E_{M_f} , which, as expected, increases as the flight path distance increases. In Fig. 3(a), we find that when the flight time is sufficiently long, the flight trajectory of the UAV tends to fly along a straight line. The flight energy consumption shown in Fig. 4(b) tends to be constant when the overall flight time becomes longer, which is consistent with the phenomenon shown in Fig. 3(a). Fig. 4(c) shows the weighted energy consumption $2w_1E_T + w_2E_{M_f}$ of the system, which is the objective function of the optimization problem. Since the $2E_T$ is much smaller than E_{M_f} , the greater w_1/w_2 is, the lower the total cost becomes. Fig. 4(c) shows that the greater the mission time, the lower the total cost. This is intuitively correct because both the data collection energy and the UAV

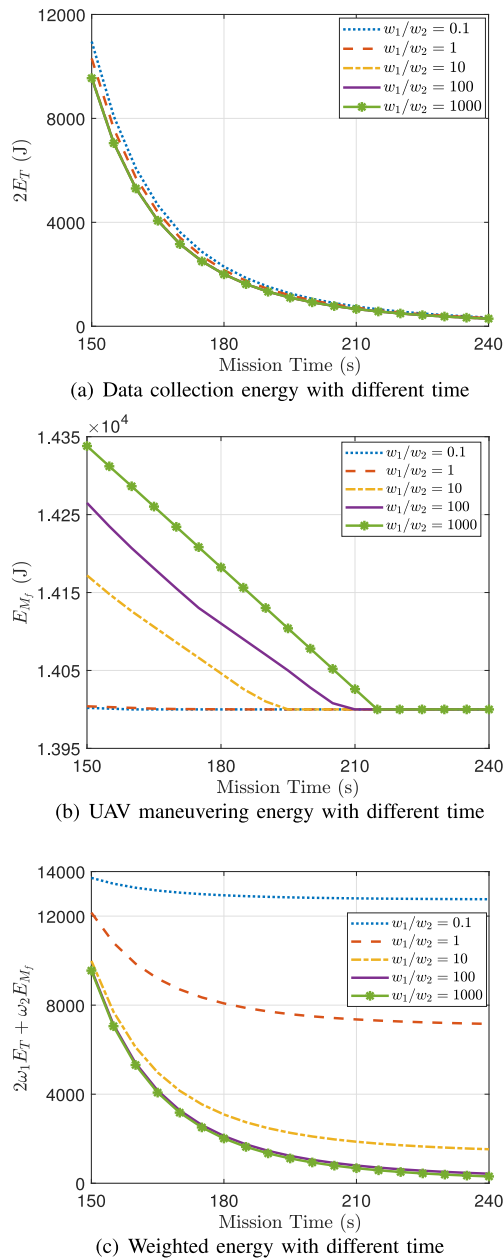


Fig. 4. The GOP characteristic parameters of the flight designed with different weighting ratios, a Gaussian distributed MTCD crowd $N(60, 60, 25, 25)$, $T = 180$ sec, $M = 50$.

flying energy decrease with the increase of the transmission time, as shown in Figs. 4(a) and 4(b).

B. Trajectories and Data Collection Performance of C-GOP and C-PSO

We now examine the C-GOP and C-PSO trajectory designs for the UAV. The parameter values are as in Table I. The environment of data transmission, the number and distribution of the MTCDs are the same as in the examples above for the GOP designs. C-GOP trajectory design divides the MTCDs into subgroups which depends on the chosen altitude of the UAV flight. The service radius of UAV depends on the flight altitude, i.e., $r_k = H/\sqrt{3}$. The C-PSO also clusters the MTCDs, but the

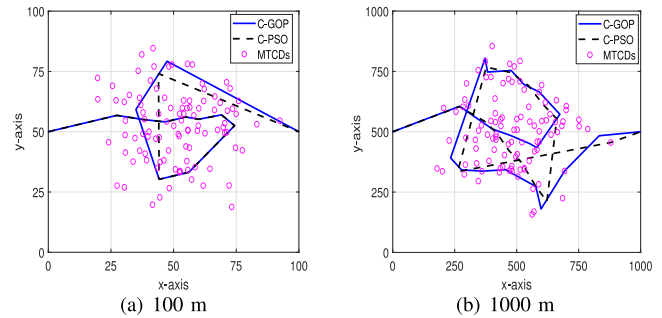
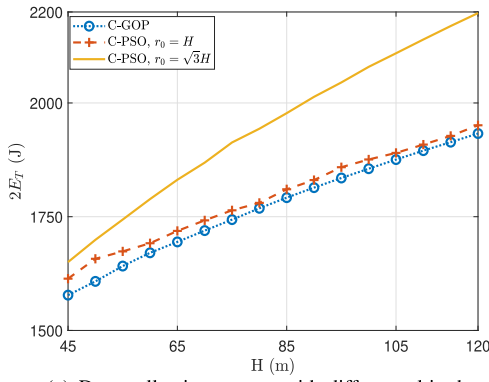


Fig. 5. C-GOP and C-PSO trajectories design for different task area size collecting data from a Gaussian distributed MTCD crowd $N(a/2, a/2, a^2/100, a^2/100)$, $M = 100$.

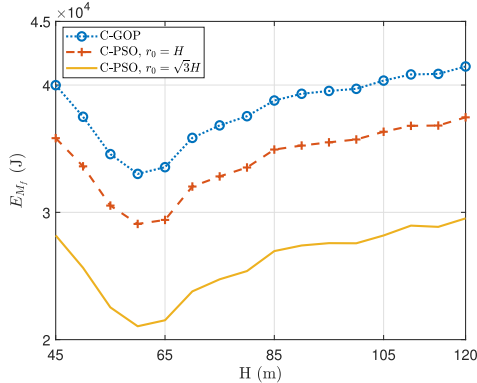
UAV's service radius does not depend on the flying altitude. The C-GOP and C-PSO strategies respectively use the GOP and PSO algorithms to find the optimal hovering points for collecting MTCD data from each sub-group. Unlike the GOP trajectory design, there is no explicit limit on the flight time for the UAV. Varying the UAV flight altitude changes the size and number of the subgroups, and thereby changes the flight path and energy the UAV consumes. The following are examples of the C-GOP and C-PSO trajectory designs under different flight altitude specifications.

Figs. 5 (a) and 5(b) show respectively the C-GOP and C-PSO trajectories for different task area sizes. It can be observed that the UAV trajectories goes straight into the center of the MTCD crowd, hovers above the position to collect data, and then flies away from the MTCD crowd to the end point.

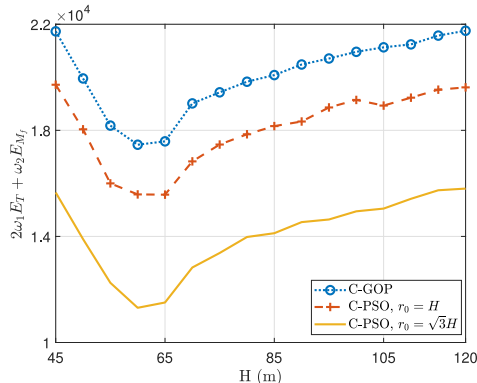
Fig. 6 shows the respective data transmission energy and flight energy for the different UAV serving radius and flight tracks at different flying altitudes. It can be observed that indeed, increasing the UAV flight altitude increases the energy consumption for data transmission. When the flying altitude of UAV increases, the service radius of UAV increases, which leads to reduced overall flying distance and flying time, and the energy consumption of UAV in flying and hovering decreases. However, as the flight altitude of the UAV continues to increase, the time required for data transmission gradually increases, and the maneuvering energy and total weighted energy consumption of the UAV also increase. From Fig. 6(c), there appears to be a flight altitude at which the flight is completed with minimum energy consumption. Under the current parameter setting, when the UAV's flying altitude is about 60 m, the total energy consumption is minimum. When the flight altitude exceeds 60 m, the total energy consumption increase slowly due to the lower data collection rate. In addition, we find that the C-GOP strategy achieved the lowest energy consumption for data transmission. This is because when the flight altitude of the UAV is fixed, the service radius of C-GOP is smaller than that of C-PSO. In addition, better in-cluster hovering points can be located by the C-GOP strategy due to the optimality nature of the GOP algorithm used, compared with the PSO algorithm. However, a smaller service radius also leads to longer service time, the UAV's maneuvering energy and total energy consumption are also larger than in the case of C-PSO.



(a) Data collection energy with different altitude



(b) UAV maneuvering energy at different altitudes

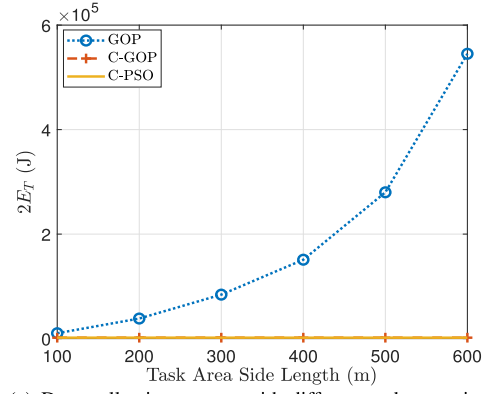


(c) Weighted energy at different altitudes

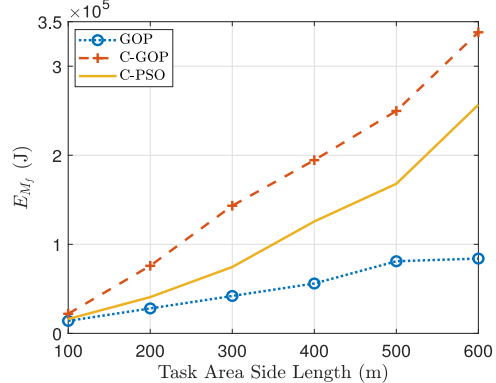
Fig. 6. The C-GOP and C-PSO characteristic parameters of the flight designed at different flying altitudes, a Gaussian distributed MTCD crowd $N(60, 60, 25, 25)$, $M = 50$.

C. Performance Comparison of GOP, C-GOP and C-PSO Algorithms

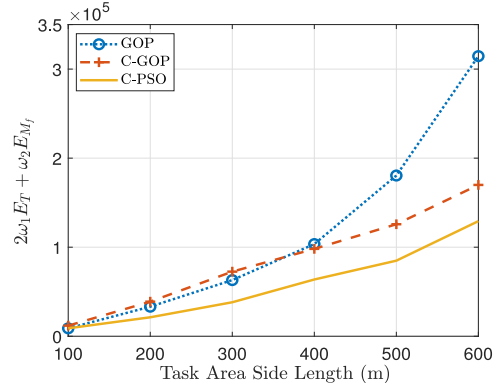
First, we observe the impact of task area size on system energy consumption. The MTCDs are Gaussian distributed physically, having the mean at $\bar{X} = a/2$ m, $\bar{Y} = a/2$ m and variances $\sigma_x^2 = \sigma_y^2 = (a^2/100)$, $\omega_1/\omega_2 = 1$. We choose r_{max} to be the distance to the MTCD farthest away from the UAV starting point. The flying time of the GOP is 180 seconds. The flying altitude of the C-GOP and C-PSO is set to $H = 60$ m. Fig. 7(a) shows that when the task area becomes larger, the energy consumption of data collection corresponding to the GOP algorithm increases rapidly. The UAV maneuvering energy consumption, as shown in Fig. 7(b),



(a) Data collection energy with different task area size



(b) UAV maneuvering energy with different task area size



(c) Weighted energy with different task area size

Fig. 7. Performance comparison of GOP, C-GOP and C-PSO algorithms with different task area size, a Gaussian distributed MTCD crowd $N(a/2, a/2, a^2/100, a^2/100)$, $M = 50$.

increases slowly. Conversely, the energy consumption of data collection corresponding to C-GOP and C-PSO algorithm increases slowly with the increase of task area, but the maneuvering energy of the UAV increase rapidly. As for the total weighted energy consumption, when the task area is small, the weighted energy consumption of the GOP algorithm is the smallest. However, as the task area gradually becomes more extensive, the weighted energy consumption of the GOP algorithm exceeds C-PSO and C-GOP. It can be observed that for larger task areas, both the C-GOP and C-PSO algorithm are more economical in energy consumption than the GOP algorithm, with the C-PSO designed trajectory having the highest energy efficiency.

TABLE II
ENERGY CONSUMPTION OF GOP WITH $B_m = 24$ Mbits, $T = 150$ s

w_1/w_2	0.1	1	10	100	1000
$(2E_T)$	2.05×10^5 J	1.97×10^5 J	1.96×10^5 J	1.95×10^5 J	1.95×10^5 J
(E_{M_f})	1.40×10^4 J	1.42×10^4 J	1.43×10^4 J	1.43×10^4 J	1.43×10^4 J
$(2w_1E_T + w_2E_{M_f})$	3.13×10^4	1.05×10^5	1.79×10^5	1.93×10^5	1.94×10^5

TABLE III
ENERGY CONSUMPTION OF GOP WITH $B_m = 24$ Mbits, $T = 180$ s

w_1/w_2	0.1	1	10	100	1000
$(2E_T)$	3.87×10^4 J	3.71×10^4 J	3.69×10^4 J	3.68×10^4 J	3.68×10^4 J
(E_{M_f})	1.40×10^4 J	1.42×10^4 J	1.43×10^4 J	1.43×10^4 J	1.43×10^4 J
$(2w_1E_T + w_2E_{M_f})$	1.63×10^4	2.56×10^4	3.48×10^4	3.67×10^4	3.69×10^4

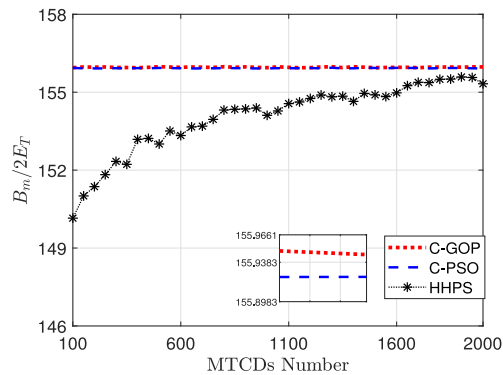


Fig. 8. Data transmission efficiency $B_m = 24$ Mbits, $\frac{w_1}{w_2} = 1$, $H = 100$ m, Distribution Area = $600\text{m} \times 600\text{m}$, a Gaussian distributed MTCD crowd $N(a/2, a/2, a^2/100, a^2/100)$.

Now we examine the efficiency of data transmission of the two clustering-based algorithms and compare it with the *hybrid hover position selection* (HHPS) algorithm in [20]. The HHPS is a clustering-based data collection algorithm aimed at minimizing the energy consumption of UAV data collection. Fig. 8 shows how the data per unit transmission energy, B_m/E_T , increases with the number of MTCDs for the three algorithms. It can be observed that while C-GOP has a slight advantage in data collection energy efficiency over C-PSO, both algorithms outperform the HHPS scheme. The HHPS uses k -medoids clustering method to cluster the ground MTCDs and determine the hovering point of the UAV. Even though this algorithm saves more energy than the traditional k -means algorithm [20], there is no optimization for the UAV's hovering point after clustering. As a result, it is outperformed by C-GOP and C-PSO algorithms where optimization was performed.

D. Special Case Study: High Density MTCD Data Collection

We examined the impact of time and task area size on the energy consumption and complexity of the designed trajectories. We now consider data collection from densely deployed MTCDs. Specifically, there are 1000 MTCDs Gaussian distributed in a 100×100 m² region, having its mean at $\bar{X} = 60$ m $\bar{Y} = 60$ m and the variances equal to $\sigma_x^2 = \sigma_y^2 = 25$. The start and the end points of the UAV

flights are fixed at $[0, 50]$ and $[100, 50]$, respectively. The information data need to be transmitted per MTCD is 24 Mbits.

1) *The GOP Performance:* (i) Applying the GOP algorithm to the scenario above for which the UAV completed the flight in $T = 150$ seconds, the energy consumption values are shown in Table II. It can be observed that for different weighting ratios w_1/w_2 , both the data transmission energy and the flying energy show little changes. However, comparing the results to those shown in Fig. 4, the energy consumption for data transmission has increased over 19 times, clearly, due to the increase of the MTCD number.

(ii) We now repeat the simulation experiment in (i) and extend the flight time to 180 seconds and examine the flight and task efficiency. Table III shows the energy consumption data of this case. Since the routes here are identical to those in case (i), the flight energy in both cases are almost unchanged, as can be observed from the figure. Besides, as in case (i), the data transmission energy hardly changes with the variation of the ratio w_1/w_2 . However, as the flight time is extended, the data transmission energy presented in Table III marked a dramatic decrease from those shown in Table II, which is consistent with the observations from Eq. (33) and Fig. 4(a).

From the above two cases, we observe that, for a larger crowd of MTCDs, the GOP design of the UAV trajectory under an over-restricted flight time demands a large amount of transmission energy, due to its high flying altitude. To reduce this transmission energy demand, the flight time must be extended. On the other hand, extending the flight time increases the computational complexity of the GOP algorithm (cf. Section III-C). Therefore, we conclude that in using the GOP trajectory, we must consider a trade-off between the design complexity and the amount of energy consumption. If a good trade-off cannot be reached such that the GOP strategy is not applicable, alternative schemes must be considered.

2) *The C-GOP and C-PSO Performance:* We now examine the C-GOP and C-PSO designs in the case of densely deployed MTCDs. Recall that both the C-GOP and C-PSO algorithms seek to divide MTCD crowd into sub-groups to collect data from each sub-group separately. Therefore, the corresponding required mission time to complete the entire task is longer, while the UAV flying altitude is much reduced. The following

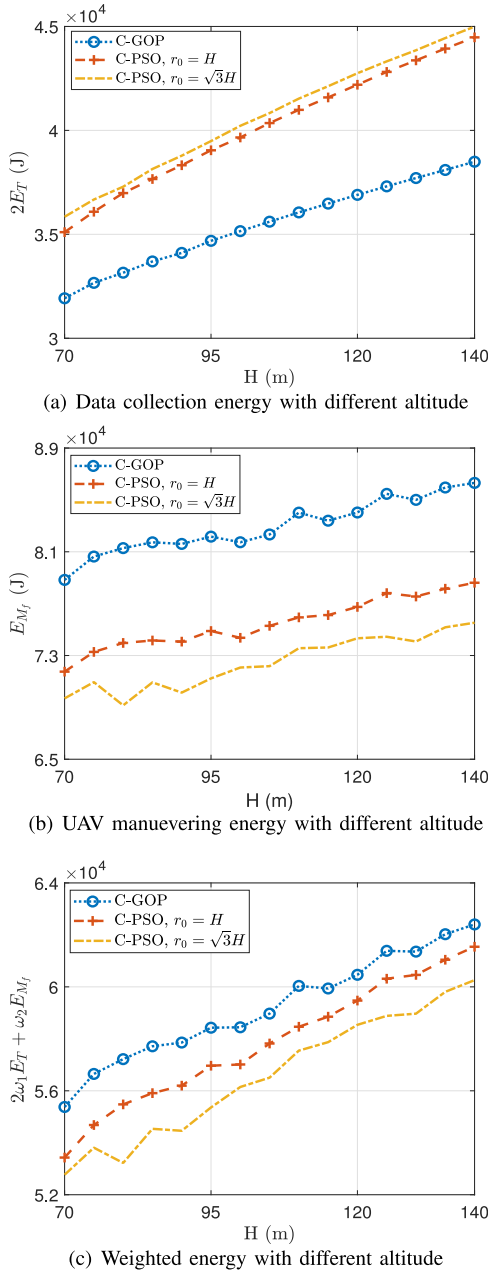


Fig. 9. Performance comparison of GOP, C-GOP and C-PSO algorithms under high-density MTCDS data collection case, a Gaussian distributed MTCDS crowd $N(60, 60, 25, 25)$, $M = 1000$.

are examples of the C-GOP and C-PSO trajectories under different flight altitude specifications.

Compared with C-PSO, the C-GOP strategy results in higher maneuvering energy consumption. It can be explained that lowering the UAV flight altitude increases flight time and hovering points, which leads to an increase in the flying and hovering energy consumption for the UAV. However, the data transmission energy consumption of the C-GOP are far less than that of the C-PSO. Comparing to the results for GOP shown in Table II, we also observed that while the C-GOP flight consumes more the flying (and hovering) energy, it consumes only about one-fifth of the data transmission energy as compared to the GOP flight. Fig. 9(c) shows the change in

total weighted energy (data transmission plus flight) with the variation of the C-GOP and C-PSO flight altitude. It can be seen that, the maneuvering energy and total weighted energy consumption of UAV increase as the flight altitude of the UAV continues to increase.

In summary, the GOP strategy gives the optimal data collection scheme when a small number of MTCDS are concentrated in a small area. When the MTCDS' density or task area size is large, the C-GOP and C-PSO algorithms are superior to the GOP algorithm for the mMTC data collection system in both total energy consumption and trajectory design complexity. As for the two clustering-based algorithms, we can say that the C-PSO can complete data collection with less UAV maneuvering energy consumption under acceptable data transmission energy efficiency. The C-GOP, on the other hand, can achieve the highest data transmission energy efficiency at the expense of a little more UAV maneuvering energy consumption.

VI. CONCLUSION

In this paper, we have studied energy-aware design of a UAV-enabled data collection scheme for an mMTC network. With the consideration of the limited energy for the UAV and MTCDS, a problem of minimizing the total energy consumption subject to completion of the data collection tasks by planning the UAV trajectory is formulated. Three data-collection strategies, designated the GOP, C-GOP, and C-PSO, respectively, have been proposed. A GOP trajectory can be obtained for a UAV serving all the MTCDS simultaneously if the UAV's flying altitude is larger than $\sqrt{3}$ times its maximum service radius. However, communication efficiency drops as the UAV's flying altitude increases. Also the complexity of the GOP algorithm sharply increases as the number of MTCDS and the UAV flying time increase. These render the applicability of the GOP algorithm limited to scenarios of small MTCDS crowds distributed over a relatively small areas. The C-GOP and C-PSO algorithms overcome such difficulties by selecting for the UAV the MTCDS within the *a priori* limited service radius to form its closest serving MTCDS set. The data collection efficiency is then maximized by optimizing the UAV hovering point for each serving MTCDS set, which is dynamically adjusted together with the UAV hovering position until all the MTCDS are served. Results from numerical experiments have confirmed that when the number of MTCDS or the task area size is large, the C-GOP and C-PSO algorithms are more favorable from energy efficiency, complexity and scalability perspectives. In particular, the C-GOP can achieve the highest data collection energy efficiency, at the expense of a little more time and UAV maneuvering energy consumption than the C-PSO strategy.

REFERENCES

- [1] W.-E. Chen, X.-Y. Fan, and L.-X. Chen, "A CNN-based packet classification of eMBB, mMTC and uRLLC applications for 5G," in *Proc. ICEA*, 2019, pp. 140–145.
- [2] S. Han, X. Xu, X. Tao, and P. Zhang, "Joint power and sub-channel allocation for secure transmission in NOMA-based mMTC networks," *IEEE Syst. J.*, vol. 13, no. 3, pp. 2476–2487, Sep. 2019.

- [3] S. Henry, A. Alsohaily, and E. S. Sousa, "5G is real: Evaluating the compliance of the 3GPP 5G new radio system with the ITU IMT-2020 requirements," *IEEE Access*, vol. 8, pp. 42828–42840, 2020.
- [4] A. C. Cirik, N. M. Balasubramanya, L. Lampe, G. Vos, and S. Bennett, "Toward the standardization of grant-free operation and the associated NOMA strategies in 3GPP," *IEEE Commun. Mag.*, vol. 3, no. 4, pp. 60–66, Dec. 2019.
- [5] N. Cheng *et al.*, "Space/aerial-assisted computing offloading for IoT applications: A learning-based approach," *IEEE J. Sel. Areas Commun.*, vol. 37, no. 5, pp. 1117–1129, May 2019.
- [6] Y. Wang *et al.*, "Joint resource allocation and UAV trajectory optimization for space–air–ground Internet of remote things networks," *IEEE Syst. J.*, vol. 15, no. 4, pp. 4745–4755, Dec. 2021.
- [7] G. Yang, R. Dai, and Y.-C. Liang, "Energy-efficient UAV backscatter communication with joint trajectory design and resource optimization," *IEEE Trans. Wireless Commun.*, vol. 20, no. 2, pp. 926–941, Feb. 2021.
- [8] F. Zhou, N. Wang, G. Luo, L. Fan, and W. Chen, "Edge caching in multi-UAV-enabled radio access networks: 3D modeling and spectral efficiency optimization," *IEEE Trans. Signal Inf. Process. Netw.*, vol. 6, pp. 329–341, Apr. 2020.
- [9] S. R. Pokhrel, J. Ding, J. Park, O.-S. Park, and J. Choi, "Towards enabling critical mMTC: A review of uRLLC within mMTC," *IEEE Access*, vol. 8, pp. 131796–131813, 2020.
- [10] C. Zhan and Y. Zeng, "Completion time minimization for multi-UAV-enabled data collection," *IEEE Trans. Wireless Commun.*, vol. 18, no. 10, pp. 4859–4872, Oct. 2019.
- [11] J. Li *et al.*, "Joint optimization on trajectory, altitude, velocity, and link scheduling for minimum mission time in UAV-aided data collection," *IEEE Internet Things J.*, vol. 7, no. 2, pp. 1464–1475, Feb. 2020.
- [12] M. Hua, L. Yang, Q. Wu, and A. L. Swindlehurst, "3D UAV trajectory and communication design for simultaneous uplink and downlink transmission," *IEEE Trans. Commun.*, vol. 68, no. 9, pp. 5908–5923, Sep. 2020.
- [13] C. Shen, T. Chang, J. Gong, Y. Zeng, and R. Zhang, "Multi-UAV interference coordination via joint trajectory and power control," *IEEE Trans. Signal Process.*, vol. 68, pp. 843–858, Jan. 2020.
- [14] Y. Wang *et al.*, "Multi-UAV collaborative data collection for IoT devices powered by battery," in *Proc. IEEE WCNC*, 2020, pp. 1–6.
- [15] L. Shen, N. Wang, Z. Zhu, Y. Fan, X. Ji, and X. Mu, "UAV-enabled data collection for mMTC networks: AEM modeling and energy-efficient trajectory design," in *Proc. IEEE ICC*, 2020, pp. 1–6.
- [16] C. Zhou *et al.*, "Deep reinforcement learning for delay-oriented IoT task scheduling in SAGIN," *IEEE Trans. Wireless Commun.*, vol. 20, no. 2, pp. 911–925, Feb. 2021.
- [17] Y. Zhang, Z. Mou, F. Gao, L. Xing, J. Jiang, and Z. Han, "Hierarchical deep reinforcement learning for backscattering data collection with multiple UAVs," *IEEE Internet Things J.*, vol. 8, no. 5, pp. 3786–3800, Mar. 2021.
- [18] S. Fu *et al.*, "Energy-efficient UAV-enabled data collection via wireless charging: A reinforcement learning approach," *IEEE Internet Things J.*, vol. 8, no. 12, pp. 10209–10219, Jun. 2021.
- [19] K. Medani, H. Guemer, Z. Aliouat, and S. Harous, "Area division cluster-based algorithm for data collection over UAV networks," in *Proc. IEEE EIT*, 2021, pp. 309–315.
- [20] K. Zhu, X. Xu, and S. Han, "Energy-efficient UAV trajectory planning for data collection and computation in mMTC networks," in *Proc. IEEE GC Wkshps*, 2018, pp. 1–6.
- [21] Y. Wang *et al.*, "Trajectory design for UAV-based Internet of Things data collection: A deep reinforcement learning approach," *IEEE Internet Things J.*, vol. 9, no. 5, pp. 3899–3912, Mar. 2022.
- [22] Y. Zeng, J. Xu, and R. Zhang, "Energy minimization for wireless communication with rotary-wing UAV," *IEEE Trans. Wireless Commun.*, vol. 18, no. 4, pp. 2329–2345, Apr. 2019.
- [23] Y. Pan, X. Da, H. Hu, Z. Zhu, R. Xu, and L. Ni, "Energy-efficiency optimization of UAV-based cognitive radio system," *IEEE Access*, vol. 7, pp. 155381–155391, 2019.
- [24] S. Boyd and L. Vandenberghe, *Convex Optimization*. Cambridge, U.K.: Cambridge Univ. Press, 2004.
- [25] Z.-H. Zhan, J. Zhang, Y. Li, and H. S.-H. Chung, "Adaptive particle swarm optimization," *IEEE Trans. Syst., Man, Cybern. B, Cybern.*, vol. 39, no. 6, pp. 1362–1381, Dec. 2009.
- [26] A. Al-Hourani, S. Kandeepan, and S. Lardner, "Optimal LAP altitude for maximum coverage," *IEEE Wireless Commun. Lett.*, vol. 3, no. 6, pp. 569–572, Dec. 2014.



Lingfeng Shen received the B.Sc. degree in applied mathematics from Zhengzhou University, Zhengzhou, China, in 2016, where he is currently pursuing the Ph.D. degree in information and communication engineering. He was a visiting Ph.D. student with the Department of Electrical and Computer Engineering, McMaster University, Canada, from 2019 to 2020, and a visiting Ph.D. student with the Department of Electrical and Computer Engineering, University of Victoria, Canada, 2018. His research interests are in wireless communications and networking, focusing on UAV communication, mobile edge computing, and machine learning.



Ning Wang (Member, IEEE) received the B.E. degree in communication engineering from Tianjin University, China, in 2004, the M.A.Sc. degree in electrical engineering from The University of British Columbia, Canada, in 2010, and the Ph.D. degree in electrical engineering from the University of Victoria, Canada, in 2013. From 2004 to 2008, he was with the China Information Technology Design and Consulting Institute as a Mobile Communication System Engineer, specializing in planning and optimization of commercial mobile communication networks. From 2013 to 2015, he was a Postdoctoral Research Fellow with the Department of Electrical and Computer Engineering, The University of British Columbia. Since 2015, he has been with the School of Information Engineering, Zhengzhou University, Zhengzhou, China, where he is currently a Professor. He also holds adjunct appointments with the Department of Electrical and Computer Engineering, McMaster University, Canada, and the State Key Laboratory of Millimeter Waves, Southeast University, China. His research interests include resource allocation and security designs of future cellular networks, channel modeling for wireless communications, statistical signal processing, and cooperative wireless communications. He was on the technical program committees of international conferences, including the IEEE GLOBECOM, IEEE ICC, IEEE WCNC, and CyberC.



Di Zhang (Senior Member, IEEE) received the Ph.D. degree from Waseda University, Tokyo, Japan, in 2017. He was a Visiting Senior Researcher with Seoul National University, Seoul, South Korea, from 2017 to 2018, and a visiting student with National Chung Hsing University, Taichung City, Taiwan, in 2012. He is currently an Associate Professor with Zhengzhou University, Zhengzhou, China, and an Adjunct Researcher with Waseda University. He has involved in two international projects in wireless communications and networking co-funded by the EU FP-7, EU Horizon 2020, and Japanese Monbusho and NICT. His research interests include wireless communications, signal processing, and the Internet of Things. In 2019, he received the ITU Young Author Award and the IEEE Outstanding Leadership Award. He is serving as an Editor for *IEEE ACCESS*, *KSII Transactions on Internet and Information Systems*, and *IET Quantum Communication*. He has served as a Guest Editor for the *IEEE WIRELESS COMMUNICATIONS*, the *IEEE NETWORK*, *IEEE ACCESS*, and *IEICE Transactions on Information and Systems*; and a TPC Member of various IEEE flagship conferences, such as ICC, GlobalSIP, WCNC, VTC, CCNC, and HEALTHCOM.



Jun Chen (Senior Member, IEEE) received the B.E. degree in communication engineering from Shanghai Jiao Tong University, Shanghai, China, in 2001, and the M.S. and Ph.D. degrees in electrical and computer engineering from Cornell University, Ithaca, NY, USA, in 2004 and 2006, respectively. From September 2005 to July 2006, he was a Postdoctoral Research Associate with the Coordinated Science Laboratory, University of Illinois at Urbana-Champaign, Urbana, IL, USA, and a Postdoctoral Fellow with IBM Thomas J. Watson Research

Center, Yorktown Heights, NY, USA, from July 2006 to August 2007. Since September 2007, he has been with the Department of Electrical and Computer Engineering, McMaster University, Hamilton, ON, Canada, where he is currently a Professor. His research interests include information theory, machine learning, wireless communications, and signal processing. He was a recipient of the Josef Raviv Memorial Postdoctoral Fellowship in 2006, the Early Researcher Award from the Province of Ontario in 2010, the IBM Faculty Award in 2010, the ICC Best Paper Award in 2020, and the JSPS Invitational Fellowship in 2021. He held the title of the Barber-Gennum Chair of Information Technology from 2008 to 2013 and the title of the Joseph Ip Distinguished Engineering Fellow from 2016 to 2018. He served as an Editor for *IEEE TRANSACTIONS ON GREEN COMMUNICATIONS AND NETWORKING* from 2020 to 2021. He is currently an Associate Editor of *IEEE TRANSACTIONS ON INFORMATION THEORY*.



Xiaomin Mu (Member, IEEE) received the B.S. degree from the Beijing Institute of Technology, Beijing, China, in 1982. She is currently a Professor Emeritus with the School of Information Engineering, Zhengzhou University, Zhengzhou. She has coauthored a number of research papers in the field of communications and signal processing. She has also coauthored two textbooks. Her research interests include signal processing in communication systems, wireless communications, and cognitive radio networks.



Kon Max Wong (Life Fellow, IEEE) received the B.Sc. (Eng.), D.I.C., Ph.D., and D.Sc. (Eng.) degrees in electrical engineering from the University of London, U.K., in 1969, 1972, 1974, and 1995, respectively. He started as a Research Engineer with the Transmission Division, Plessey Telecommunications Research Ltd., U.K., in 1969. In October 1970, he was on leave from Plessey pursuing postgraduate studies and research with the Imperial College of Science and Technology, London. In 1972, he rejoined Plessey as a Principal

Research Engineer and worked on digital signal processing and signal transmission. In 1976, he joined the Department of Electrical Engineering, Technical University of Nova Scotia, Canada, and in 1981, moved to McMaster University, Hamilton, Canada, where he has been a Professor since 1985 and served as a Chairman of the Department of Electrical and Computer Engineering from 1986 to 1987, from 1988 to 1994, and from 2003 to 2008. He was on leave as a Visiting Professor with the Department of Electronic Engineering, The Chinese University of Hong Kong from 1997 to 1999. He currently holds the Principal Chair Professorship with Zhengzhou University, China, and is a Professor Emeritus with McMaster University. His research interest is in signal processing and communication theory and has published over 250 papers in the area. He was a recipient of the IEE Overseas Premium for the Best Paper in 1989, and is also coauthored papers that received the IEEE Signal Processing Society Best Young Author awards of 2006 and 2008. He was awarded a Distinguished Visiting Fellowship by the Royal Academy of Engineering, U.K., in 2009, was a recipient of the Alexander Von Humboldt Research Award in 2010 and the McMaster Faculty of Engineering Life-Time Research Achievement Award in 2011. He was an Associate Editor of the *IEEE TRANSACTIONS ON SIGNAL PROCESSING* from 1996 to 1998 and served as a Chair of the Sensor Array and Multi-Channel Signal Processing Technical Committee of the IEEE Signal Processing Society from 2002 to 2004. He has also been an Elected Fellow of the Canadian Academy of Engineering as well as a Fellow of the Royal Society of Canada. He is a Fellow of the Institution of Electrical Engineers, Royal Statistical Society, and Institute of Physics.